

Article

Effect of Cu on the Fracture and Exfoliation Corrosion Behavior of Al-Zn-Mg-xCu Alloy

Huibin Jiao ^{1,2}, Kanghua Chen ^{1,2,3,*}, Songyi Chen ^{1,2,*}, Zhen Yang ^{1,2}, Peng Xie ^{1,3} and Shanda Chen ^{1,3}

¹ Light Alloy Research Institute, Central South University, Changsha 410083, China; jhb20140101@163.com (H.J.); yangzhen0@csu.edu.cn (Z.Y.); xp1475774217@163.com (P.X.); xiaoxiannv@163.com (S.C.)

² Science and Technology on High Strength Structural Materials Laboratory, Central South University, Changsha 410083, China

³ Collaborative Innovation Center of Advance Nonferrous Structural Materials and Manufacturing, Central South University, Changsha 410083, China

* Correspondence: Khchen@csu.edu.cn or 15073175702@163.com (K.C.); Sychen08@csu.edu.cn (S.C.); Tel.: +86-731-8883-0714 (S.C.)

Received: 2 November 2018; Accepted: 3 December 2018; Published: 11 December 2018



Abstract: In the present work, the influence of Cu content on microstructure, mechanical properties and exfoliation corrosion behaviors of Al-Zn-Mg-xCu alloy extrusions has been investigated in longitudinal-transverse (L-T) and short-longitudinal (S-L) directions by means of mechanical tensile and exfoliation corrosion testing combined with optical microscopy (OM), scanning electron microscopy (SEM) and transmission electron microscopy (TEM). The results showed that a higher Cu content significantly decreased the fracture toughness and ductility of the alloy in S-L direction compared with L-T direction. Concomitant with the increase in Cu content, a transition in fracture mode was observed from transgranular dimpled rupture to intergranular rupture in S-L direction. Moreover, the exfoliation corrosion (EXCO) resistance of the alloy decreased as the Cu content increased and the exfoliation corrosion resistance of the alloy in short-transverse (S-T) direction was better than that of L-T direction. These results were mainly associated with the large number of coarse intermetallics caused by high Cu content in the L-T direction of alloy.

Keywords: Al-Zn-Mg-Cu aluminum alloy; Cu; anisotropy; exfoliation corrosion resistance

1. Introduction

Nowadays, the 7xxx series of aluminum alloys have been widely applied in the aerospace industry, profiting from their excellent combination of low density, high specific strength and high toughness [1,2]. With the rapid development of the aerospace industry and the innovation of science and technology, the demand for large-scale structural parts of high strength Al-Zn-Mg-Cu aluminum alloy is more urgent. Aiming at the requirements of large-scale, integrated, lightweight and high-reliability of aerospace aluminum alloy structural parts, it is urgent to develop high-strength, high-toughness and thick-section aluminum alloy materials with low anisotropy and high hardenability to realize the integration of large and complex aluminum structural parts [3,4].

At present, the typical Al-Zn-Mg-Cu aluminum alloys for the production of large-size thick plates and forgings are 7050 and 7085 aluminum alloys. For example, the 7050-T7451 pre-stretched thick plates are used as fuselage frame, longeron, empennage and so forth, of the aircraft, which have been widely used in the US fourth-generation fighters F22, F35 and Boeing 777 aircraft. 7085-T7452 forgings have been successfully applied to important bearing members such as longeron and landing gears in

Boeing 787 and Airbus A380 aircraft [5–7]. With the development of aerospace industry, the demand for large-sized cross-section components (especially thick plates) is becoming more and more urgent and the requirements such as hardenability and mechanical property uniformity of the alloy are also becoming stricter [8–10]. Wu et al.'s research showed that the anisotropy of fatigue crack propagation was ascribed to the coarse inclusion particles and T_1 precipitates [11]. Jata et al. suggested that the yield stress anisotropy may be due to the combined synergistic effect of particles and crystallographic texture [12]. Hu et al. showed that the occurrence of the anisotropy in over-aged 7050 aluminum alloy was mainly attributed to the microstructures, which were further characterized by visible precipitate free zones (PFZs) and coarse precipitates in (sub)grain boundaries [13]. However, there are few studies on the influence of alloy composition on the anisotropy of mechanical properties for Al-Zn-Mg-Cu aluminum alloy thick plate or forging, such as the Cu element. As the main alloying element of Al-Zn-Mg-Cu alloy, Cu has its solid solution strengthening effect and its addition could change the precipitation phase structure of the alloy and make the aging precipitates more dispersed and uniform, which could improve the strength and plasticity of the alloy. However, as the content of Cu increases, the alloy will have a problem of high corrosion sensitivity. Marlaud et al. observed that the precipitates were easy coarsening in the lower Cu-containing alloy due to slower diffusivity of Cu in Al compared to Mg and Zn atoms [14]. Knight et al. believed that the reduction of quenching rate contributed to the increase of Cu content in grain boundary, thereby improving the stress corrosion resistance [15]. It has also been reported that the increase of Cu content in the alloy would lead to an increase in the number of intermetallics and a decrease in the corrosion resistance of the alloy [16].

In this work, Al-Zn-Mg-xCu aluminum alloys were used as the research object to study the effect of Cu content on the microstructure, mechanical properties anisotropy and corrosion properties of Al-Zn-Mg-xCu alloys. Our aim is to provide guidance for improving the comprehensive properties of Al-Zn-Mg-Cu aluminum alloy plate or forging.

2. Materials and Methods

Al-Zn-Mg-Cu alloy were prepared by a casting metallurgy method and the chemical compositions were measured by inductively coupled plasma optical emission spectroscopy (ICP-OES, Huaxu, Beijing, China) and the results were showed in Table 1. The ingot was graded homogenization annealing in a resistance air furnace: it was kept at 410 °C for 4 h, subsequently heated to 475 °C for 24 h at a heating rate of 0.8 °C/min and air-cooled. The samples were subjected to multidirectional forging at 430 °C with a compression speed of 5 mm/s by using a 5 MN numerically-controlled hydraulic press (YH27-500T, Hefei Forging Machine Co., Ltd., Hefei, China). In each upset forging process, the specimens were compressed along different axes with a height reduction of 50%. The principle of multi-directional forging could refer to reference [17], which includes 6 instances of upset forging, 6 instances of stretch-forging and 1 instance of shape-forging to obtain the final forging of 150 mm × 60 mm × 50 mm. The extrusion deformation was carried out on a 500 t press, the size of the extrusion nozzle was 50 mm × 50 mm and the extrusion speed was appropriately controlled to ensure the uniformity of the deformed structure. The samples were solution treated at 470 °C for 1 h, quenched in room temperature water and undergone three-step aging (110 °C, 6 h) + (160 °C, 8 h, water quenching) + (120 °C, 24 h, air cooling), then the alloy structure was observed and the mechanical properties and corrosion performance were analyzed.

Table 1. The chemical compositions of alloys (wt.%).

Alloys	Zn	Mg	Cu	Ti	Zr	Al
0.98 wt.%Cu	7.60	1.60	0.98	0.028	0.129	Bal.
1.45 wt.%Cu	7.66	1.64	1.45	0.027	0.129	Bal.
1.69 wt.%Cu	7.63	1.62	1.69	0.028	0.129	Bal.
2.02 wt.%Cu	7.64	1.61	2.02	0.028	0.129	Bal.

The alloy was sampled as shown in Figure 1 with longitudinal-transverse (L-T) along the extrusion direction and short-transverse (S-T) in the vertical extrusion direction. The structure of alloy was observed in a DM4000M (Leica, Wizz, German) intelligent microscope. The fracture morphology after stretching at room temperature was measured using a JSM-6360 (JEOL, Tokyo, Japan) LV scanning electron microscope (SEM). The atomic ratio of the elements in the second phase was determined by energy spectrum analysis (EDS, Apollo XP, AMETEK, Berwyn, PA, USA) to determine the type of the second phase. The microstructures of the alloy were observed under a JEM-2100F (JEOL, Tokyo, Japan) transmission electron microscope (TEM).

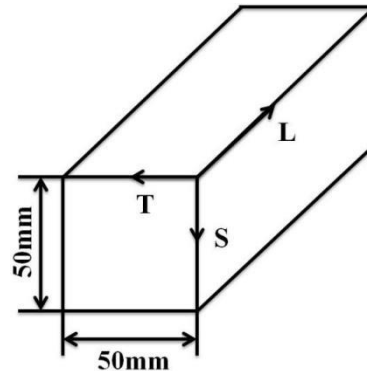


Figure 1. Sampling direction of the test specimen.

The fracture toughness test is performed according to GB4161-2007 standard. Mechanical properties test was performed on a smooth specimen by a CSS-44100 testing machine at room temperature with tensile speed of 2 mm/min. The specimen was extracted from 1/2 position of the extrusion bar for testing. In the test, five times of tensile tests were carried out for each Cu content alloy.

The EXCO test was performed according to GB/22639-2008 standard and the corrosive medium was a standard EXCO solution (4 mol/L NaCl + 0.4 mol/L KNO₃ + 0.1 mol/L HNO₃ in 25 ± 1 °C). After immersing for 24 h, the sample was rinsed with water and the surface corrosion product was removed with a 30% nitric acid solution, subsequently washed with water, dried and the corrosion grade was evaluated according to the national standard. In the EXCO experiment, each Cu content alloy was subjected to 3 tests.

3. Results

3.1. Optical Microstructure

Figure 2 shows the optical microstructure of the samples with different Cu content. It could be seen that after plastic deformation, the L-T direction grain of the alloy is elongated (Figure 2a–d) and the coarse intermetallics is mainly distributed along the deformation direction at the grain boundary or subgrain boundary. However, the S-T direction grain structure of the alloy is disc-shaped (Figure 2e–h) and the intermetallics is randomly distributed. There are almost no intermetallics in the alloy when the Cu content is 0.98 wt.% (Figure 2a,e). Instead, there are many coarse black intermetallics in the alloy when the Cu content is 2.02 wt.% (Figure 2d–h). Moreover, the degree of recrystallization in the L-T and S-T directions increases with the Cu content increases.

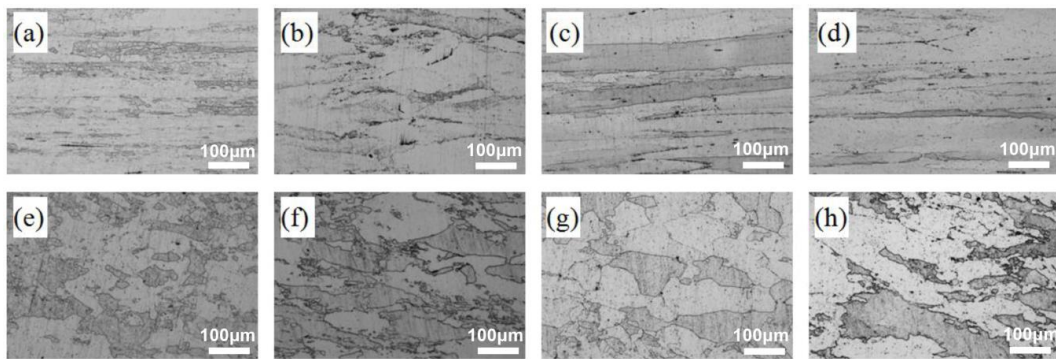


Figure 2. Optical micrographs of the aged alloys: (a,e) 0.98 wt.%Cu; (b,f) 1.45 wt.%Cu; (c,g) 1.69 wt.%Cu; (d,h) 2.02 wt.%Cu; L-T: (a–d); S-T: (e–h).

3.2. Second Phase Analysis

Figure 3 shows the SEM morphology of the intermetallics (the second phase) in different Cu content alloys. Table 2 shows the count, average area and area fraction analysis of the second phase in the alloy. Figure 3 and Table 2 analysis show that the number and size of intermetallics in the L-T and S-T directions all increase with the increase of Cu content but there are some differences in the distribution. The intermetallics of L-T direction changes from discrete distribution to chain distribution, whereas the intermetallics in S-T direction are randomly distributed. Energy spectrum analysis for the 2.02 wt.%Cu alloy shows that the phase rich in Cu and Fe is Al_7Cu_2Fe and the phase rich in Cu and Mg is $S (Al_2CuMg)$ (Figure 4).

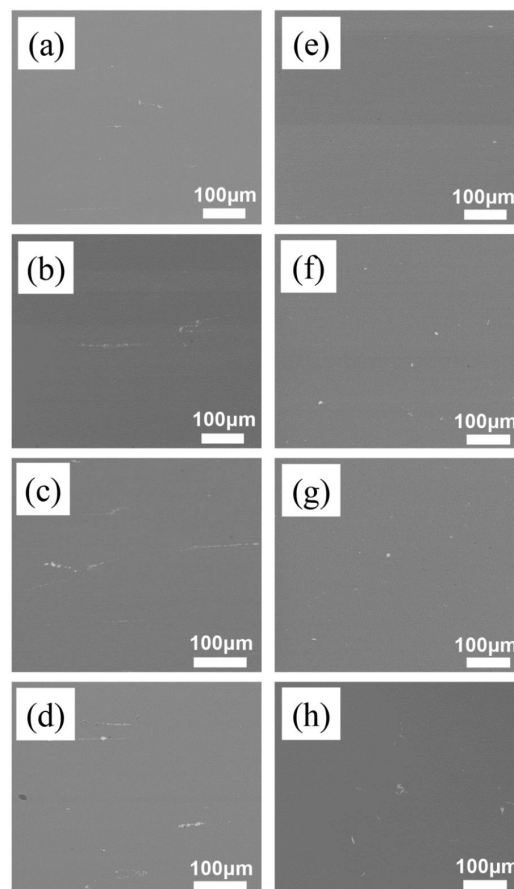
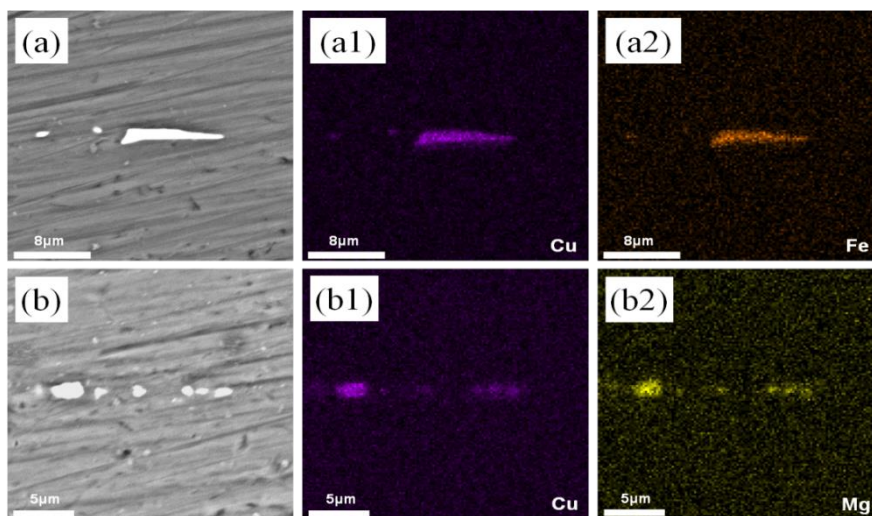


Figure 3. SEM images of the alloys with different Cu contents: (a,e) 0.98 wt.%Cu; (b,f) 1.45 wt.%Cu; (c,g) 1.69 wt.%Cu; (d,h) 2.02 wt.%Cu; L-T: (a–d); S-T: (e–h).

Table 2. Analysis of the count, average area and area fraction of second phase in the alloy.

Alloys	Count	Average Area (μm^2)	Area (%)
0.98 wt.%Cu (L-T)	205	1.34	0.11
0.98 wt.%Cu (S-T)	241	1.33	0.09
1.45 wt.%Cu (L-T)	244	1.51	0.17
1.45 wt.%Cu (S-T)	312	1.48	0.12
1.69 wt.%Cu (L-T)	314	1.68	0.26
1.69 wt.%Cu (S-T)	349	1.63	0.22
2.02 wt.%Cu (L-T)	363	2.01	0.34
2.02 wt.%Cu (S-T)	353	1.79	0.27

**Figure 4.** EDS element spectrum of the second phase for 2.02 wt.%Cu alloy: (a,a1,a2) $\text{Al}_7\text{Cu}_2\text{Fe}$; (b,b1,b2) Al_2CuMg .

3.3. TEM Observation

Figure 5 shows the TEM morphology of the aged alloy and Table 3 displays the results of grain boundary precipitation (GBP) microstructure feature of the alloys. We can see that the average size, area fraction and spacing of the GBP all increase as the Cu content increases. Moreover, the size of the GBP in S-T direction is larger and the precipitation free zone (PFZ) in S-T direction is wider compared with that of L-T direction.

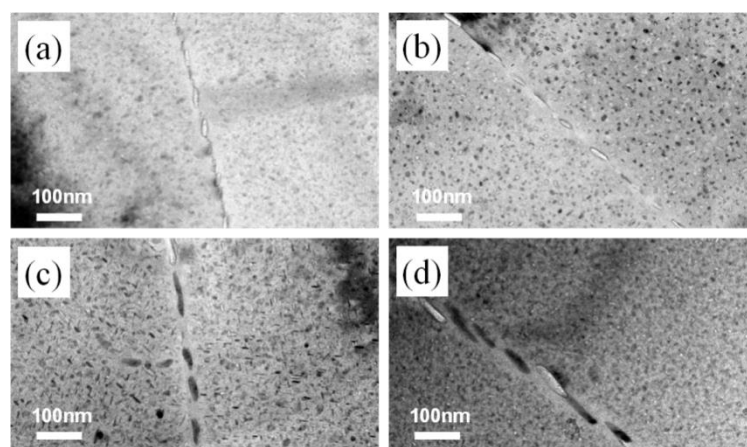
**Figure 5.** TEM images of the alloys: (a) 0.98 wt.%Cu (L-T); (b) 0.98 wt.%Cu (S-T); (c) 2.02 wt.%Cu (L-T); (d) 2.02 wt.%Cu (S-T).

Table 3. Summary of data showing grain boundary microstructures of the alloys.

Alloys	PFZ Width (nm)	GBPs Size (nm)	GBPs A _f (%)
0.98 wt.%Cu (L-T)	24.7 ± 2.2	15.4 ± 3.2	17.2 ± 1.5
0.98 wt.%Cu (S-T)	27.2 ± 1.6	15.7 ± 3.0	17.9 ± 1.9
2.02 wt.%Cu (L-T)	28.1 ± 1.6	26.1 ± 3.4	23.6 ± 1.8
2.02 wt.%Cu (S-T)	31.4 ± 1.9	26.7 ± 2.7	24.8 ± 2.4

3.4. Fracture Toughness

The fracture toughness test is performed according to GB4161-2007 standard. In the test, five times of tensile tests are carried out for each Cu content specimen. Figure 6a shows the data of fracture toughness with error bars and Figure 6b is the data of plane anisotropy index (IPA) of the alloys with different Cu contents. Figure 6a indicates that the fracture toughness of the alloy in the L-T/S-L directions first increases and then decreases when the Cu contents increase from 0.98 wt.% to 2.02 wt.% and the fracture toughness of the alloy in the L-T/S-L directions reach the maximum values of 35.4/30.8 MPa·m^{1/2} when the Cu content is 1.45 wt.%. Moreover, the IPA values gradually increase with the Cu contents increase (Figure 6b) and the IPA reaches a minimum value of 9.6% when the Cu content is 0.98 wt.%. Here, the IPA is defined according to reference [18]:

$$IPA = (X_{\max} - X_{\min}) / X_{\max} \times 100\% \quad (1)$$

where X_{\max} and X_{\min} represent the maximum and minimum values of fracture toughness, respectively.

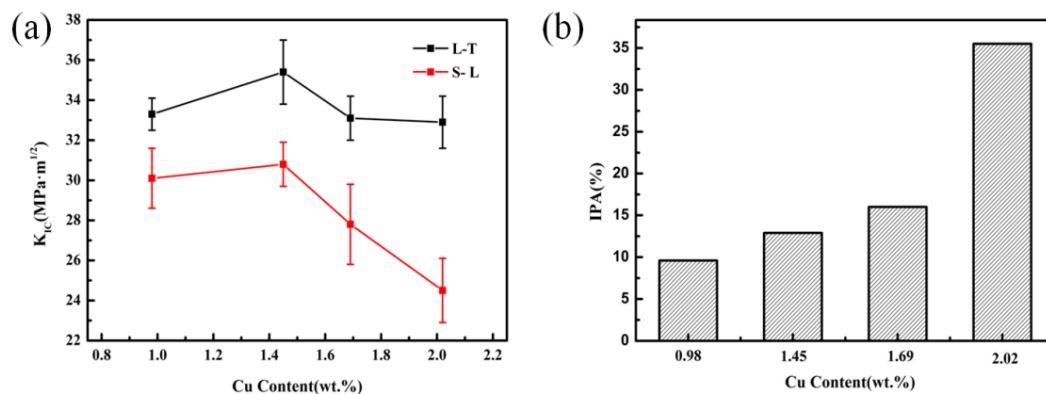


Figure 6. Fracture toughness and IPA of the alloys with different Cu contents: (a) Fracture toughness; (b) IPA.

3.5. Fracture Morphology

Figure 7 shows the SEM fracture morphologies of the alloys with different Cu contents. Figure 7a–d show the fracture morphology of the alloy in L-T direction, we can see that the dimples of transgranular fracture in the alloy are obviously shallow in depth, smaller and uneven in size with the increase of Cu content and the proportion of intergranular fracture also increases. A large amount of small dimples present with the Cu content of 0.98 wt.% and when the Cu content reaches to 1.45 wt.%, transgranular fracture is dominant in the alloy. When the Cu content is 1.69 wt.% or 2.02 wt.%, the fracture mode (fracture morphology) of the alloy is still a composited but intergranular fracture begins to dominate and the fracture morphology appears plateau.

Figure 7e–h are the S-L direction fracture morphology of the alloys. It could be seen that a transition in fracture mode is observed from transgranular dimpled fracture to intergranular fracture with the increase of Cu contents. When the Cu content is 0.98 wt.% and 1.45 wt.%, the main fracture mode of the alloy is transgranular fracture and the fracture morphology consists of large and deep dimples. While, when the Cu content reaches to 1.69 wt.% or 2.02 wt.%, intergranular fracture is

dominant and the dimples are very few and shallow and the fracture edges are distributed parallel to each other along the L-T direction.

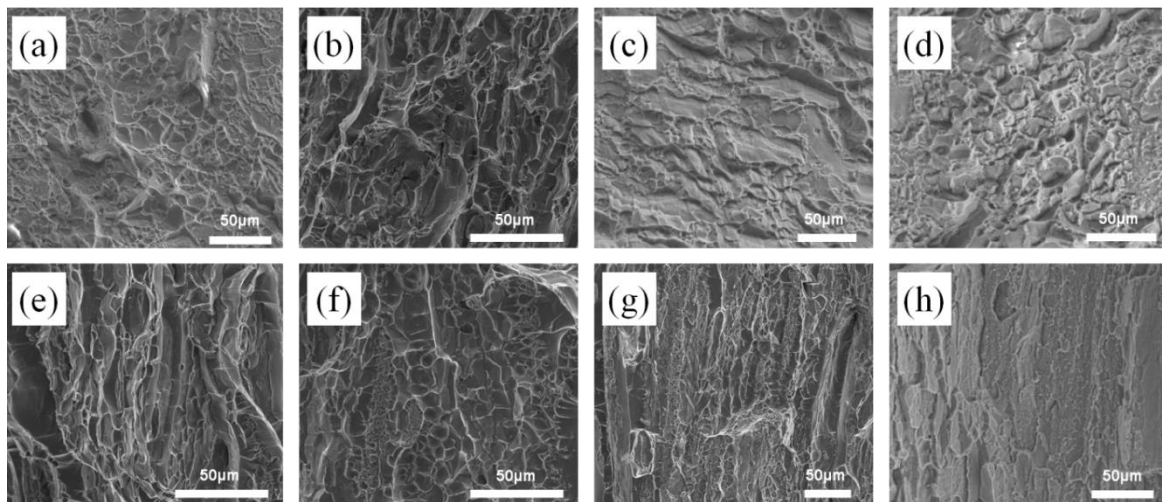


Figure 7. SEM images of the fracture morphology of the alloys: (a,e) 0.98 wt.%Cu; (b,f) 1.45 wt.%Cu; (c,g) 1.69 wt.%Cu; (d,h) 2.02 wt.%Cu; L-T: (a–d); S-L: (e–h).

3.6. The Exfoliation Corrosion Behavior

The evolution of the visual ratings in the EXCO experiments are carried out on the four alloys according to GB/T 22639-2008 and the results are shown in Figure 8. It could be seen that the exfoliation corrosion resistance of the alloys decreases as the Cu content increases. Figure 9 shows the exfoliation corrosion morphology of the alloys with different Cu contents after immersing for 24 h. Figure 9a,e indicate that only a slight metal peeling occurs in the L-T direction of the alloy with the Cu content of 0.98 wt.%, which could be evaluated as PC. Meanwhile, the metal has slight pitting accompanied with a small amount of metal blasting in the S-T direction, which is rated as PB. When the content of Cu increases to 2.02 wt.%, the alloy is severely corrosive and layered and the corrosion penetrates deep into the metal, which is evaluated as EC in both L-T and S-T directions. It is worth noting that all alloys have better S-T direction corrosion resistance than L-T direction.

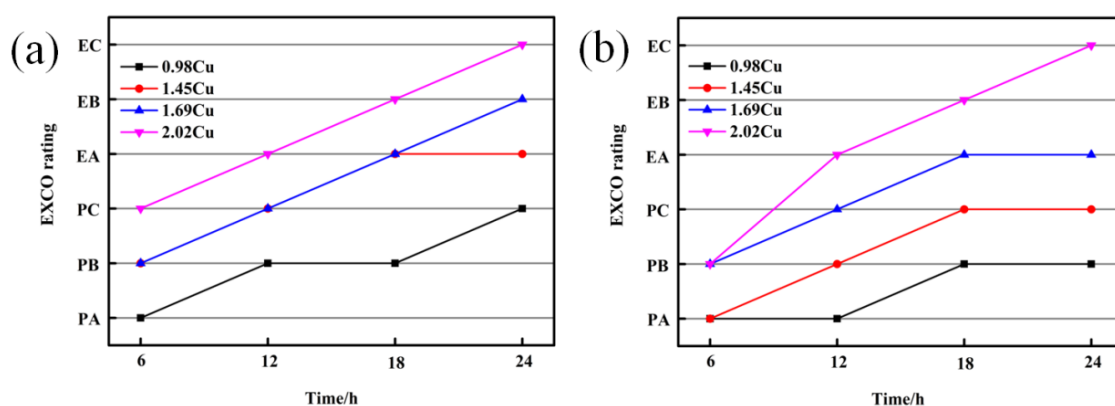


Figure 8. Variation of EXCO rating for alloys during immersing in the EXCO solution for 24 h: (a) L-T; (b) S-T.

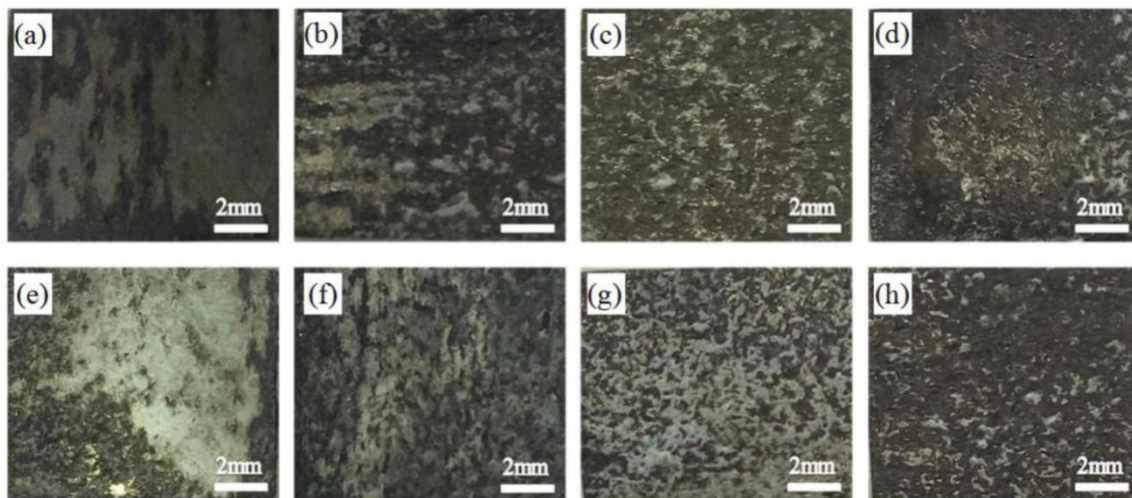


Figure 9. Morphologies of exfoliation corrosion of the alloys with different Cu contents: (a,e) 0.98 wt.%Cu; (b,f) 1.45 wt.%Cu; (c,g) 1.69 wt.%Cu; (d,h) 2.02 wt.%Cu; L-T: (a–d); S-T: (e–h).

4. Discussion

4.1. Effect of Cu on Fracture of Alloy

Al-Zn-Mg-Cu alloy is a typical aged-hardenable alloy. Precipitation strengthening caused by strengthening phases such as η' phase and GP zone during aging can enhance the strength of the alloy [6,19]. A small amount of Cu can promote the precipitation of strengthening phase but when the content of Cu increases to a certain extent ($\text{Cu} > 1.45$ wt.%), the formed $\text{S}(\text{Al}_2\text{CuMg})$ phase will consume the Mg element, which would result in the decrease of the η' phase formation and the adverse effect on the alloy strength [20]. Therefore, the fracture toughness of the alloy first increases and then decreases as the Cu content ranges from 0.98 wt.% to 2.02 wt.% (Figure 6). Furthermore, as shown in Figure 4, the volume fraction of the second phase increases with the Cu content increase. These second phase have the characteristics of high hardness, high brittleness, low strength and are easily deformed and cracked, which could reduce the local plastic deformation ability of the alloy matrix, thereby reducing the mechanical properties of the alloy.

In the L-T direction tensile fracture morphology of the alloy, the dimples of transgranular fracture are obviously shallow in depth, smaller and uneven in size with the increase of Cu content and the proportion of intergranular fracture increases (Figure 7a–d). When the Cu content reaches to 2.02 wt.%, the main fracture mode of the alloy is intergranular fracture accompanied with fewer transgranular fracture and the fracture morphology appears platform. When the alloy is stretched in L-T direction, the crack propagation appears in the S-T plane and the GB area in this plane is relatively large. In addition, the GB are not in a plane in the S-T direction, resulting in a larger interplanar spacing of GB. The coarse intermetallic particles are mainly distributed inside the grains of the alloy. When the tensile stress is applied, the micropores first appear inside the grains to form a transgranular fracture. When the crack propagation direction is perpendicular to the direction of the intermetallic particles (Figure 4), the resistance of crack propagation is large, which leads the crack propagation tend to shift in the direction of low resistance, resulting the improvement of alloy strength and fracture toughness.

A transition in fracture mode is observed from transgranular dimpled fracture to intergranular fracture with the increase of Cu contents in S-L direction (Figure 7e–h). Figure 7e shows the characteristic of transgranular dimpled fracture and small dimples exist in large dimples. When the Cu content increases to 2.02 wt.%, the dimples are almost disappeared with the generation of plateau and the tearing edges are parallel to the L-T direction, which is due to that the volume fraction of the intermetallics increases with the increase of Cu content. As the coarse intermetallic particles have low strength and weak interfaces, the dislocations accumulates around these coarse intermetallic particles,

which make the stress concentrated and preferentially crack of the coarse particles [21]. Therefore, increasing the volume fraction of the coarse particles would decrease the fracture toughness and ductility of the alloy. When the sample is tensile in the S-L direction, the crack propagation plane is the L-T plane. When the crack propagation direction coincides with the arrangement direction of the intermetallic particles, the resistance of crack propagation is small, which leads to the easy formation of the “fracture path.” Therefore, the S-L direction mechanical properties of the alloy are poor.

4.2. Effect of Cu on Exfoliation Corrosion

It is known that EXCO is actually a kind of intergranular corrosion (IGC) and closely associated with grain shape. For pitting corrosion, it is widely accepted that metastable pits occurred around larger intermetallic particles are more easily to turn into stable pits, since the larger and deeper cavity provided a longer diffusion barrier and a more severe acidification as a result of hydrolysis of metal ions [22]. In general, the EXCO of Al-Zn-Mg-Cu alloys are also originated from pitting, therefore larger size of iron and copper rich intermetallic particles would promote the continuous growth of corrosion pits and hence the occurrence of EXCO. Therefore, the corrosion resistance of the alloy decreased as the Cu content increased due to high content of intermetallics. The potential of GBPs in Al-Zn-Mg-Cu alloy is about -0.8 to -1.0 V_{sce}, which is obviously negative compared with Al matrix of -0.68 V_{sce}. However, the added Cu element will be partially dissolved in GBPs and the potential of the alloy will be raised to reduce the potential difference with the matrix, which is beneficial to the corrosion resistance of the alloy [3,15]. Meanwhile, with the Cu content increases, the amount of residual intermetallics also increase (Figure 3 and Table 2), which could cause a relative decrease in the Cu content of matrix, thereby increasing the potential difference with the matrix. Generally, the potential difference tends to become the driving force of corrosion galvanic couples for the alloy in the corrosive medium, which will accelerate the occurrence of intergranular corrosion. Besides, Figure 4 and Table 3 indicate the discontinuous distribution of precipitates on the grain boundaries or widening of the PFZ may be beneficial to the improvement of the corrosion resistance of the alloys [10].

The results of the exfoliation corrosion grades of alloys with different Cu contents in L-T and S-T directions are shown in Figure 8. It can be seen that the degree of exfoliation corrosion of the alloys with different Cu contents is different and the corrosion surfaces of the same alloy in different directions are also different. As can be seen from Figure 3, there is a significant difference in grain morphology between L-T and S-T directions. The grain structure of the alloy in the L-T direction is oriented fiber deformation. While the grain structure in the S-T direction is equiaxed and the grain boundaries are not elongated with large density. EXCO usually occurs in a strong acid environment and the corrosion gradually progresses along the fibrous grains, leading to surface spalling [8]. Figure 10 shows the secondary electron images of the SEM surface morphology for 1.45 wt.%Cu alloy after immersion in EXCO solution for 24 h. We can see that the corrosion paths of the alloy are different in the L-T/S-T directions. The results are consistent with the study by Song et al., they reported that the corrosion resistance of the S-T plane is enhanced compared with that of the L-T and S-L planes due to approximately equiaxed the grain structure in the S-T plane [23]. Moreover, as the Cu content increases, the coarse intermetallic particles in the alloy increases (as shown in Figure 4) and the corrosion resistance of the alloy decreases. However, it is worth noting that the EXCO corrosion resistance of alloy in S-T direction is better than that of L-T direction.

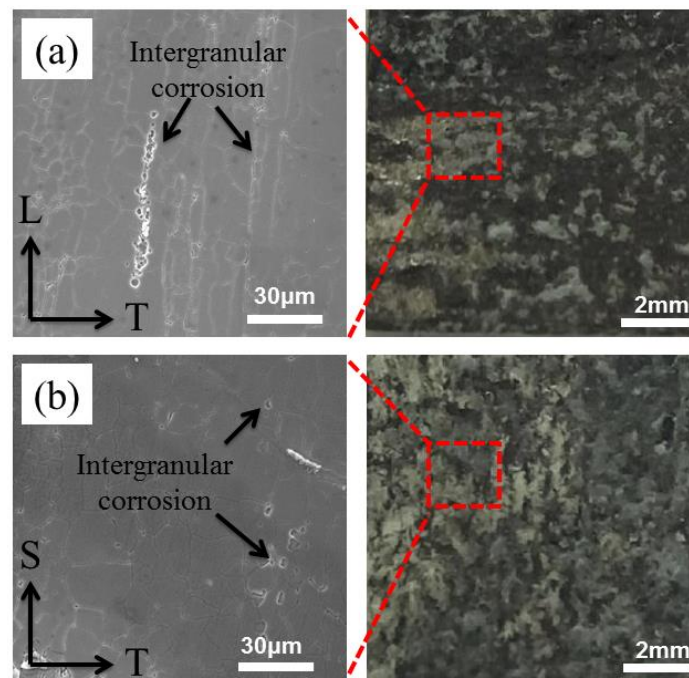


Figure 10. Secondary electron images of the SEM surface morphology of 1.45 wt.%Cu alloy after immersion in EXCO solution for 24 h: (a) L-T; (b) S-T.

5. Conclusions

The tests of mechanical tensile and exfoliation corrosion were conducted on the Al-Zn-Mg-xCu aluminum alloys to investigate the effect of Cu contents on the fracture toughness and exfoliation corrosion behaviors of the alloy and the main results are as follows.

- (1) The amount of intermetallics in the L-T and S-T directions of the alloy all increases with the increase of Cu content. The intermetallics of L-T direction accumulate at the grain boundary along the deformation direction, whereas the intermetallics in S-T direction are discretely distributed.
- (2) The fracture toughness of the alloy in L-T and S-L directions all increases first and then decreases with the increase of Cu contents and the maximum fracture toughness of the alloy is 1.45 wt.%.
- (3) The fracture mode is transformed from transgranular dimpled rupture to intergranular rupture in S-L direction with the increase of Cu contents.
- (4) The EXCO corrosion resistance of the alloy decreases as the Cu content increases and the EXCO corrosion resistance of the alloy in S-T direction is better than that of L-T direction.

Author Contributions: H.J., S.C. and K.C. conceived and designed the experiments; H.J. carried out the experiments; H.J. analyzed the data; Z.Y., P.X. and S.C. contributed reagents, materials and analysis tools; and H.J. wrote the paper.

Funding: This research was funded by National Key Research and Development Program of China (No. 2016YFB0300801), Major Research Equipment Development Projects of National Natural Science Foundation of China (No. 51327902).

Conflicts of Interest: The authors declare no conflict of interest.

References

1. Zuo, J.R.; Hou, L.G.; Shi, J.T.; Hua, C.; Zhuang, L.Z.; Zhang, J.H. The mechanism of grain refinement and plasticity enhancement by an improved thermomechanical treatment of 7055 Al alloy. *Mater. Sci. Eng. A* **2017**, *702*, 42–52. [[CrossRef](#)]
2. Liu, S.D.; Li, Q.; Lin, H.Q.; Sun, L.; Long, T.; Ye, L.Y.; Deng, Y.L. Effect of quench-induced precipitation on microstructure and mechanical properties of 7085 aluminum alloy. *Mater. Des.* **2017**, *132*, 119–128. [[CrossRef](#)]

3. Knight, S.P.; Pohl, K.; Holroyd, N.J.H.; Birbilis, N.; Rometsch, P.A.; Muddle, B.C.; Goswami, R.; Lynch, S.P. Some effects of alloy composition on stress corrosion cracking in Al-Zn-Mg-Cu alloys. *Corros. Sci.* **2015**, *98*, 50–62. [[CrossRef](#)]
4. Huo, W.T.; Shi, J.T.; Hou, L.G.; Zhang, J.S. An improved thermo-mechanical treatment of high-strength Al-Zn-Mg-Cu alloy for effective grain refinement and ductility modification. *J. Mater. Process. Technol.* **2017**, *239*, 303–314. [[CrossRef](#)]
5. Fang, H.C.; Luo, F.H.; Chen, K.H. Effect of intermetallic phases and recrystallization on the corrosion and fracture behavior of an Al-Zn-Mg-Cu-Zr-Yb-Cr alloy. *Mater. Sci. Eng. A* **2017**, *684*, 480–490. [[CrossRef](#)]
6. Fang, H.C.; Chao, H.; Chen, K.H. Effect of recrystallization on intergranular fracture and corrosion of Al-Zn-Mg-Cu-Zr alloy. *J. Alloys Compd.* **2015**, *622*, 166–173. [[CrossRef](#)]
7. Wen, K.; Xiong, B.Q.; Zhang, Y.A.; Wang, G.J.; Li, X.W.; Li, Z.H.; Huang, S.H.; Liu, H.W. Microstructure Evolution of a High Zinc Containing Al-Zn-Mg-Cu Alloy during Homogenization. *Rare Met. Mater. Eng.* **2017**, *46*, 928–934.
8. Marlaud, T.; Malki, B.; Henon, C.; Deschamps, A.; Baroux, B. Relationship between alloy composition, microstructure and exfoliation corrosion in Al-Zn-Mg-Cu alloys. *Corros. Sci.* **2011**, *53*, 3139–3149. [[CrossRef](#)]
9. Yan, Z.; Xiao, W.L.; Ge, S.J.; Zhao, W.T.; Hanada, S.J.; Ma, C.L. Effect of Cu content and Cu/Mg ratio on the microstructure and mechanical properties of Al-Si-Cu-Mg alloys. *J. Alloys Compd.* **2015**, *649*, 291–296.
10. Liu, S.D.; Chen, B.; Li, C.B.; Dai, Y.; Deng, Y.L.; Zhang, X.M. Mechanism of low exfoliation corrosion resistance due to slow quenching in high strength aluminium alloy. *Corros. Sci.* **2015**, *91*, 203–212. [[CrossRef](#)]
11. Wu, W.T.; Liu, Z.Y.; Bai, S.; Li, F.D.; Liu, M.; Wang, A. Anisotropy in fatigue crack propagation behavior of Al-Cu-Li alloy thick plate. *Mater. Charact.* **2011**, *131*, 440–449. [[CrossRef](#)]
12. Jata, K.V.; Panchanadeeswaran, S.; Vasudevan, A.K. Evolution of texture, microstructure and mechanical property anisotropy in an Al-Li-Cu alloy. *Mater. Sci. Eng. A* **1998**, *257*, 37–46. [[CrossRef](#)]
13. Hu, H.; Wang, X.Y. Effect of Heat Treatment on the In-Plane Anisotropy of As-Rolled 7050 Aluminum Alloy. *Met.-Basel* **2018**, *6*, 79. [[CrossRef](#)]
14. Marlaud, T.; Deschamps, A.; Bley, F.; Lefebvre, W.; Baroux, B. Influence of alloy composition and heat treatment on precipitate composition in Al-Zn-Mg-Cu alloys. *Acta Mater.* **2010**, *58*, 248–260. [[CrossRef](#)]
15. Knight, S.P.; Birbilis, N.; Muddle, B.C.; Trueman, A.R.; Lynch, S.P. Correlations between intergranular stress corrosion cracking, grain-boundary microchemistry, and grain-boundary electrochemistry for Al-Zn-Mg-Cu alloys. *Corros. Sci.* **2010**, *52*, 4073–4080. [[CrossRef](#)]
16. Chen, S.Y.; Chen, K.H.; Dong, P.X.; Ye, S.P.; Huang, L.P. Effect of heat treatment on stress corrosion cracking, fracture toughness and strength of 7085 aluminum alloy. *Trans. Nonferrous Met. Soc. China* **2014**, *24*, 2320–2325. [[CrossRef](#)]
17. He, H.L.; Yi, Y.P.; Huang, S.Q.; Zhang, Y.X. Effects of deformation temperature on second-phase particles and mechanical properties of 2219 Al-Cu alloy. *Mater. Sci. Eng. A* **2018**, *712*, 414–423. [[CrossRef](#)]
18. Shen, F.H.; Yi, D.Q.; Jiang, Y.; Wang, B.; Liu, H.L.; Tang, C.; Shou, W.B. Semi-quantitative evaluation of texture components and fatigue properties in 2524 T3 aluminum alloy sheets. *Mater. Sci. Eng. A* **2016**, *657*, 15–25. [[CrossRef](#)]
19. Deng, Y.; Yin, Z.M.; Cong, F.G. Intermetallic phase evolution of 7050 aluminum alloy during homogenization. *Intermetallics* **2012**, *26*, 114–121. [[CrossRef](#)]
20. Rodríguez, J.J.S.; Hernández, F.J.S.; Juan, E.G.G. The effect of environmental and meteorological variables on atmospheric corrosion of carbon steel, copper, zinc and aluminium in a limited geographic zone with different types of environment. *Corros. Sci.* **2003**, *45*, 799–815. [[CrossRef](#)]
21. Robinson, J.S.; Cudd, R.L.; Tanner, D.A.; Dolan, G.P. Quench sensitivity and tensile property inhomogeneity in 7010 forgings. *J. Mater. Process. Technol.* **2001**, *119*, 261–267. [[CrossRef](#)]
22. She, H.; Chu, W.; Shu, D.; Wang, J.; Sun, B.D. Effects of silicon content on microstructure and stress corrosion cracking resistance of 7050 aluminum alloy. *Trans. Nonferrous Met. Soc. China* **2014**, *24*, 2307–2313. [[CrossRef](#)]
23. Song, F.X.; Zhang, X.M.; Liu, S.D.; Han, N.M.; Li, D.F. Anisotropy of localized corrosion in 7050-T7451 Al alloy thick plate. *Trans. Nonferrous Met. Soc. China* **2014**, *23*, 2483–2490. [[CrossRef](#)]

